

# A Scalable Gaussian Process for Large-Scale Periodic Data

Yongxiang Li, Yuting Pu

Department of Industrial Engineering and Management,  
Shanghai Jiao Tong University, Shanghai, China.

Changming Cheng

State Key Laboratory of Mechanical System and Vibration,  
Shanghai Jiao Tong University, Shanghai, China.

Qian Xiao\*

Department of Statistics,  
University of Georgia, Athens, GA, USA

## Abstract

The periodic Gaussian process (PGP) has been increasingly used to model periodic data due to its high accuracy. Yet, computing the likelihood of PGP has a high computational complexity of  $\mathcal{O}(n^3)$  ( $n$  is the data size), which hinders its wide application. To address this issue, we propose a novel circulant PGP (CPGP) model for large-scale periodic data collected at grids that are commonly seen in signal processing applications. The proposed CPGP decomposes the log-likelihood of

---

\*Contact: Qian Xiao, qian.xiao@uga.edu, 310 Herty Dr, Department of Statistics, University of Georgia, Athens, GA, USA, 30602.

PGP into the sum of two computationally scalable composite log-likelihoods, which do not involve any approximations. Computing the likelihood of CPGP requires only  $\mathcal{O}(p^2)$  (or  $\mathcal{O}(p \log p)$  in some special cases) time for grid observations, where the segment length  $p$  is independent of and much smaller than  $n$ . Simulations and real case studies are presented to show the superiority of CPGP over some state-of-the-art methods, especially for applications requiring periodicity estimation. This new modeling technique can greatly advance the applicability of PGP in many areas and allow the modeling of many previously intractable problems.<sup>1</sup>

**Keywords:** Hypothesis testing, Periodic signals, Noise resistant correlation function, Periodicity estimation, Optimization.

## 1 Introduction

Periodic data, such as speech signals (Nielsen et al., 2017), electrocardiogram (ECG) signals (Chandola and Vatsavai, 2011), and vibration signals (Fan et al., 2018), are commonly encountered in scientific research and industrial applications. Such signals are often analyzed via linear models, e.g., the maximum likelihood pitch estimation (MLPE) method (Wise et al., 1976) and the noise resistant correlation (NRC) method (Li et al., 2021), or nonlinear models, e.g., the nonlinear least square (NLS) method (Quinn and Thomson, 1991; Nielsen et al., 2017). These methods can provide desirable estimations and predictions in many applications, but they become less accurate when handling signals with a low signal-to-noise ratio (SNR) and may require very long signals to suppress the masking effect of strong background noises (Fan et al., 2018; Li et al., 2021). A key reason is that they do not appropriately model the circulant within-period correlation of periodic data, i.e., the autocorrelation between any two points in one period.

The periodic Gaussian process (PGP) has been increasingly used in recent years, espe-

---

<sup>1</sup>Supplementary materials for this article are available online.

cially for modeling signals under strong noise environments. It can well model the circulant within-period correlation and thus significantly improve the performance (Zhang et al., 2005; Chandola and Vatsavai, 2011). For example, Chandola and Vatsavai (2011) proposed a PGP-based change point detection for the online monitoring of periodic time series, which has superior performance compared with many current methods. Durrande et al. (2016) adapted the framework of PGP to detect the periodicity in the Arabidopsis genome, and Guérin et al. (2020) developed a robust object detection based on PGP filtering. Koulali and Clarke (2021) proposed to use PGP for modeling geodetic time series to estimate the secular velocity of selected GPS sites. PGP has also been used for long-term forecasting of periodic processes and periodic error control (HajiGhassemi and Deisenroth, 2014; Klenske et al., 2015).

Despite its advantage in accuracy, PGP faces two challenges that hinder its wide application. First, computing the likelihood of PGP requires a high complexity of  $\mathcal{O}(n^3)$ , where  $n$  is the signal length. It can be prohibitively slow when dealing with moderate or large-scale data, e.g., spending several hours to process 10,000 data points on a normal computer. Second, PGP often requires a known period or treats it as a tuning parameter. Yet, in real applications, the true period is often unknown, and periodicity detection is often of key interest. The current literature lacks efficient methods for estimating periods in PGP, which is a challenging optimization problem involving numerous local optimums.

To address the challenge on computation, various approximation methods in the current GP literature may be adopted, which can be summarized as follows. One strategy is to simplify the covariance structure of GP, including low-rank GP (Cressie and Johannesson, 2008; Stein, 2008), inducing-point GP (Quinonero-Candela and Rasmussen, 2005; Titsias, 2009), local GP (Choudhury et al., 2002; Park et al., 2011), covariance tapering (Kaufman et al., 2008; Bevilacqua et al., 2016), and sparse GP (Snelson and Ghahramani, 2007; Sang and Huang, 2012). Another strategy is to approximate the full likelihood of GP via the conditional composite likelihood (Vecchia, 1988; Stein et al., 2004; Katzfuss and Guinness,

2021) or block marginal composite likelihood (Caragea and Smith, 2007; Eidsvik et al., 2014). All these approximation methods may be applied to PGP, but they will inevitably suffer from a certain amount of information loss and thus sacrifice some model accuracy for computational convenience. Moreover, most of these methods are not scalable, and their computational complexity still depends on the data size. Please refer to Section 2 for a thorough review.

In signal processing applications, data are often collected using a given sampling frequency at grids. That is, the time series are equally spaced. In dealing with such data, some algebraic methods based on circulant and Toeplitz covariance structure may be used to accelerate GP without any approximations. The embedding circulant matrix (Wood and Chan, 1994; Coeurjolly and Porcu, 2018) is a popular method for fast and exact simulations from GPs. Yet, the covariance matrix of PGP may not be circulant because the signal length  $n$  may not always be multiples of the segment length  $p$ . So far, the Toeplitz-based PGP (TPGP) is the most efficient method in the literature that does not involve approximations in calculating likelihoods (Zhang et al., 2005; Chandola and Vatsavai, 2011). It can accelerate the computational complexity of  $\mathcal{O}(n^3)$  in PGP to  $\mathcal{O}(n^2)$ . Yet, this approach may still be prohibitively slow when dealing with large-scale data.

To address the two challenges in classic PGP methods, we propose a novel circulant PGP (CPGP) model for large-scale periodic data collected at grids. The proposed CPGP divides the entire data into  $k$  segments and a remaining part if  $n$  is not multiples of  $k$ . It decomposes the log-likelihood of PGP into the sum of two computationally scalable composite log-likelihoods, which accelerates the computational complexity for calculating likelihoods from  $\mathcal{O}(n^3)$  in PGP to  $\mathcal{O}(p^2)$  in CPGP, where the segment length  $p$  is independent of and much smaller than the data size  $n$ . When  $p$  divides  $n$ , it can be further improved to  $\mathcal{O}(p \log p)$ . Note that CPGP has exactly the same likelihoods as PGP given the period, and thus it does not involve any approximations compared to PGP.

Different from classic PGP methods requiring known periods, the proposed estimation

of CPGP includes a tailored optimization algorithm that can efficiently estimate periods if they are not known in advance. Considering the cost of searching unknown periods in CPGP, the total computational complexity for model fitting is  $\mathcal{O}(d^3 p_{max}^3)$ , where  $p_{max}$  is the largest searching length for  $p$  and  $d$  is a tuning parameter controlling the decimal precision of period estimations. Additionally, we also show that CPGP provides the exact prediction as the best linear unbiased prediction (BLUP) in PGP, and its computational complexity is  $\mathcal{O}(p^2)$ . It clearly outperforms classic composite likelihood predictors that may suffer from non-negligible information loss (Eidsvik et al., 2014). Above all, the likelihood calculation, model fitting, and model prediction in CPGP are all scalable, and no approximation is needed unlike those for PGP.

When periodic data are collected at grids, the proposed CPGP should be used wherever PGP models are applicable. It enables the use of the accurate PGP framework to real applications that have large-scale data or unknown periods. Notably, we do not advocate the use of CPGP for data that are not collected at grids. Compared with some state-of-the-art non-GP methods, including NLS (Nielsen et al., 2017), NRC (Li et al., 2021), and MLPE (Wise et al., 1976), CPGP performs better when dealing with low SNR, such as vibration signals, and at the same time, is computationally efficient. Besides the computational efficiency for handling long signals, CPGP is particularly useful for fast and accurate periodicity detection, i.e., accurately identifying the periods within a very short time using a moderate number of data. Although CPGP is designed for strictly periodic signals, it can also be used for analyzing pseudo-periodic signals, which is illustrated in real case studies. Additionally, we discuss an approximate version of CPGP in the simulation study, which is faster but generally performs worse than CPGP.

The remainder of this article is organized as follows. In Section 2, we briefly review the current literature on GP, PGP, and some non-GP methods for modeling periodic data. In Section 3, we detail the likelihood formulation, parameter estimation, and model prediction of the scalable CPGP. In Section 4, a simulation study on synthetic periodic signals is

presented to evaluate the performance of CPGP. In Section 5, two real case studies are discussed to illustrate the superiority of CPGP. In Section 6, we conclude this study and discuss some further work. All proofs and additional technical details are relegated to Supplementary Materials.

## 2 Brief Literature Review

GP is a stochastic process where every finite collection of random variables indexed by time or space follows a multivariate normal distribution. The GP model, also known as Kriging, was first developed in the field of geostatistics (Sacks et al., 1989) and then became widely used in many areas of science and engineering (Fang et al., 2006; Gramacy, 2020). It can learn from temporal and/or spatial correlations and provide desirable performance. Mathematically, the GP model (i.e. universal Kriging) can be defined as

$$y(t) = \mathbf{f}^T(t) \boldsymbol{\beta} + z(t) + \epsilon(t), \quad (1)$$

where  $\mathbf{f}(t)$  is a regression function,  $\boldsymbol{\beta}$  is a vector of coefficients,  $z(t)$  is a zero mean GP with the variance  $\sigma^2$  and stationary correlation function  $\varphi_\phi(t, t')$  ( $\phi$  is the vector of parameters in the function), and  $\epsilon(t) \sim \mathcal{N}(0, \sigma^2 \delta^2)$  is an i.i.d. noise.

The parameters in the GP model ( $\phi$ ,  $\boldsymbol{\beta}$ ,  $\sigma^2$ , and  $\delta^2$ ) are often obtained with maximum likelihood estimation (MLE, Santner et al. 2013), i.e., by maximizing the following log-likelihood function (up to a constant)

$$\ell(\phi, \boldsymbol{\beta}, \sigma^2, \delta) = -\frac{\log |\sigma^2 \mathbf{K}_\delta| + \frac{(\mathbf{y} - \mathbf{F}\boldsymbol{\beta})^T \mathbf{K}_\delta^{-1} (\mathbf{y} - \mathbf{F}\boldsymbol{\beta})}{\sigma^2}}{2}, \quad (2)$$

where  $\mathbf{F} = [\mathbf{f}(t_1), \dots, \mathbf{f}(t_n)]^T$  is the regression matrix, and  $\sigma^2 \mathbf{K}_\delta$  is the covariance matrix of the GP. Here, the covariance  $\mathbf{K}_\delta = \mathbf{K} + \delta^2 \mathbf{I}_n$ , where the correlation matrix  $\mathbf{K}$  is calculated from  $n$  sample points according to a chosen correlation function  $\varphi_\phi(t, t)$ .

With the partial derivatives of the log-likelihood in Eq. (2) equated to zero, the parameter estimates of  $\boldsymbol{\beta}$  and  $\sigma^2$  are

$$\begin{cases} \hat{\boldsymbol{\beta}} &= (\mathbf{F}^T \mathbf{K}_\delta^{-1} \mathbf{F})^{-1} \mathbf{F}^T \mathbf{K}_\delta^{-1} \mathbf{y} \\ \hat{\sigma}^2 &= \frac{1}{n} (\mathbf{y} - \mathbf{F} \hat{\boldsymbol{\beta}})^T \mathbf{K}_\delta^{-1} (\mathbf{y} - \mathbf{F} \hat{\boldsymbol{\beta}}) \end{cases}. \quad (3)$$

Then, we can obtain the profile likelihood for the MLE of  $\phi$  and  $\delta$ , which is to solve the minimization problem  $\hat{\phi}, \hat{\delta} = \text{minimize}_{\phi, \delta} \{n \log \hat{\sigma}^2 + \log |\mathbf{K}_\delta|\}$  via some searching algorithms. Given parameter estimates, the model prediction can be made through BLUP

$$\hat{y}(t) = \mathbf{f}^T(t) \hat{\boldsymbol{\beta}} + \mathbf{r}^T(t) \mathbf{K}_\delta^{-1} (\mathbf{y} - \mathbf{F} \hat{\boldsymbol{\beta}}), \quad (4)$$

where the correlation vector  $\mathbf{r}(t) = [\varphi_{\hat{\phi}}(t, t_1), \dots, \varphi_{\hat{\phi}}(t, t_n)]^T$ . Additionally, we have its variance as  $\text{Var}(\hat{y}(t)) = \sigma^2(1 - \mathbf{r}^T(t) \mathbf{K}_\delta^{-1} \mathbf{r}(t) + \boldsymbol{\omega}^T (\mathbf{F}^T \mathbf{K}_\delta^{-1} \mathbf{F})^{-1} \boldsymbol{\omega})$ , where  $\boldsymbol{\omega} = \mathbf{f}(t) - \mathbf{F}^T \mathbf{K}_\delta^{-1} \mathbf{r}(t)$ . More details on GP derivations can be found in Santner et al. (2013) and Gramacy (2020).

Many usual correlation functions, e.g., Gaussian and Matern kernels, may not be appropriate for modeling periodic data, because they do not consider the periodic dependency. In the PGP literature, the periodic correlation function proposed by MacKay (1998) is widely used, which is defined as

$$\psi_\phi(t, t') = \exp\left(-\theta^2 \sin^2\left(\frac{\pi(t - t')}{T}\right)\right), \quad (5)$$

where  $\phi = \{\theta, T\}$ ,  $\theta$  is the roughness (length scale) parameter, and  $T$  is the period. The correlation function in Eq. (5) can well model the circulant correlation structure of periodic data, and the correlation between the beginning and end points within any period converges to one. More discussions and examples can be found in Rasmussen and Williams (2006).

Model fitting and prediction for the GP model, including PGP, require calculating the

inverse and determinant of the covariance matrix, both having a computational complexity of  $\mathcal{O}(n^3)$ . For moderate or large datasets, it can be very time consuming. In practice, periodic data, such as speech, ECG, and vibration signals, often include more than 100,000 data points, and fitting a classic GP or PGP is almost impossible for such data sizes.

To speed up GP methods, one common strategy is to simplify the covariance structure via some approximations. For example, low-rank GP (Cressie and Johannesson, 2008; Stein, 2008; Finley et al., 2009; Xiong, 2021) was proposed to approximate the correlation matrix  $\mathbf{K}$  by constructing the factorization  $\mathbf{K} \approx \mathbf{Q}_{n \times p} \mathbf{K}_{p \times p}^{-1} \mathbf{Q}_{n \times p}^T$ , where  $\mathbf{K}_{p \times p}$  is the correlation matrix of  $p$  inducing points (Quinonero-Candela and Rasmussen, 2005; Titsias, 2009). It can accelerate the computational complexity of GP to  $\mathcal{O}(np^2)$ . Additionally,  $\mathbf{K}_{p \times p}$  was rendered circulant by Tebbutt et al. (2016) for pseudo-circular GP approximation, which will further reduce the computational complexity to  $\mathcal{O}(np \log p)$ . Moreover, local approximations (Choudhury et al., 2002; Park et al., 2011) for large-scale GP were proposed by fitting local GP models on a subset of data. Covariance tapering (Kaufman et al., 2008; Bevilacqua et al., 2016) was proposed by utilizing a sparse covariance structure for computational convenience. Sparse GP (Snelson and Ghahramani, 2007; Sang and Huang, 2012) was developed to combine the low-rank and local GP. Another strategy is to apply divide-and-conquer with composite likelihoods. Specifically, composite likelihoods were used to approximate the full likelihood of GP for parameter estimation (Vecchia, 1988; Heagerty and Lele, 1998; Stein et al., 2004; Caragea and Smith, 2007) and model prediction (Eidsvik et al., 2014). A sequential pairwise modeling approach (Li and Zhou, 2016) was developed to achieve excellent scalability for multivariate GPs.

All these GP approximations can be applied to PGP, though most of them have not been implemented in the current literature. One challenge is that they may have non-negligible information loss due to approximations, thereby affecting the accuracy of PGP. In signal processing applications, periodic data are often collected at grids. For such data, the embedding circulant matrix method (Wood and Chan, 1994; Davies and Bryant, 2013)

can be used to scale GP without any approximations, where the Toeplitz covariance matrix of GP can be embedded into a circulant covariance matrix. Calculating the inverse and determinant of the covariance matrix requires  $\mathcal{O}(n \log n)$  and  $\mathcal{O}(n^2)$  time, respectively, and thus the complexity of computing likelihoods is  $\mathcal{O}(n^2)$  (Zhang et al., 2005; Chandola and Vatsavai, 2011). This method has been successfully applied to GP simulations (Dietrich and Newsam, 1997; Coeurjolly and Porcu, 2018) and log-Gaussian Cox processes (Diggle et al., 2013; Taylor and Diggle, 2014).

Specifically, TPGP proposed by Chandola and Vatsavai (2011) is currently the most efficient PGP dealing with periodic data collected at grids, i.e.,  $t_i = i/f_s$ , where  $f_s$  is the sampling frequency. Its covariance matrix  $\sigma^2 \mathbf{K}_\delta$  is proved to be a Toeplitz matrix (diagonal-constant matrix) for any period  $T$ , because any  $i$ th and  $j$ th element of the correlation matrix  $\mathbf{K}$  is

$$\psi_\phi(t_i, t_j) = \exp\left(-\theta^2 \sin^2\left(\frac{\pi(i/f_s - j/f_s)}{T}\right)\right). \quad (6)$$

Clearly, all descending diagonals of  $\mathbf{K}$  are constant, and so is  $\mathbf{K}_\delta = \mathbf{K} + \delta^2 \mathbf{I}_n$ . Then, a Toeplitz matrix inversion algorithm (Trench, 1964) can be used to accelerate the computation of likelihoods in  $\mathcal{O}(n^2)$  time.

The proposed CPGP differs from current GP (or PGP) methods in the following four aspects. First, different from all GP (or PGP) approximation methods, CPGP has exactly the same likelihood as PGP for periodic data collected at grids, thus maintaining the same accuracy. Second, CPGP is a scalable approach that requires only  $\mathcal{O}(p^2)$  time (or  $\mathcal{O}(p \log p)$  in a special case) for calculating likelihoods, where  $p$  is independent of and much smaller than  $n$ . In contrast, most current GP methods are still not scalable even after acceleration, e.g., low rank GP and TPGP have a computational complexity of  $\mathcal{O}(np \log p)$  and of  $\mathcal{O}(n^2)$ , respectively. Third, CPGP can handle the case where  $n$  is not multiples of  $p$ , while current methods based on circulant matrices cannot, though they all leverage fast Fourier transform (FFT) to accelerate the computation. Fourth, unlike current PGP

methods that commonly assume known periods, the estimation of CPGP includes an efficient optimization for identifying unknown periods. Note that besides GP-based methods, we will also compare the proposed CPGP with some state-of-the-art non-GP methods, including fast NLS (FNLS, Nielsen et al. 2017), NRC (Li et al., 2021), and MLPE (Wise et al., 1976), via numerical studies.

### 3 Circulant Periodic Gaussian Process

Large-scale periodic data are often collected at grids by using a given sampling frequency in signal processing applications. To enable an accurate PGP framework for modeling such data, we propose a scalable modeling approach, called CPGP, which is fast in both parameter estimation and model prediction. Following the settings in Zhang et al. (2005) and Chandola and Vatsavai (2011), we assume the periodic data are collected at grids with the sampling frequency  $f_s$  and the period can be written as  $T = p/(df_s)$ , where  $p$  and  $d$  are co-prime integers. The tuning parameter  $d$  is used to allow a decimal number of points (i.e.,  $p/d$  points) in one period and control the estimation accuracy of  $T$ . In practice, the sampling frequency  $f_s$  for collecting data is often given, while the true period  $T$  of the signal is often unknown. By plugging  $T = p/(df_s)$  into Eq. (6), the correlation function  $\psi_\phi(t_i, t_j)$  can be written as

$$\psi_\phi(t_i, t_j) = \exp\left(-\theta^2 \sin^2\left(\frac{\pi d(i-j)}{p}\right)\right), \quad (7)$$

where  $i, j = 1, \dots, n$  and  $\phi = \{\theta, p, d\}$ .

#### 3.1 Exact Likelihood Decomposition

In CPGP, we divide the periodic signal collected at grids into  $k = \lfloor n/p \rfloor$  segments, each having  $p$  data points, where  $\lfloor n/p \rfloor$  denotes the maximum integer not greater than  $n/p$ . The

$r$ th segment is denoted as  $\mathbf{y}_r = [y(t_{(r-1)p+1}), \dots, y(t_{rp})]^T$  for  $r = 1, 2, \dots, k$ , and the remaining data points that cannot form a segment are denoted as  $\mathbf{y}_* = [y(t_{kp+1}), \dots, y(t_n)]^T$ .

A key novelty of CPGP is that it decomposes the log-likelihood  $\ell$  in PGP into the sum of two computationally scalable composite log-likelihoods without any approximations. Specifically, by applying the conditional probability, we have

$$\ell(\theta, \delta, p, d) = \ell_1 + \eta \ell_2, \quad (8)$$

where  $\ell_1 = \log \Pr(\mathbf{y}_1, \dots, \mathbf{y}_k)$  is the log-likelihood of  $\mathbf{y}_1, \dots, \mathbf{y}_k$ ,  $\ell_2 = \log \Pr(\mathbf{y}_* | \mathbf{y}_1, \dots, \mathbf{y}_k)$  is the log-likelihood of  $\mathbf{y}_*$  conditional on  $\mathbf{y}_1, \dots, \mathbf{y}_k$ , and  $\eta = 0$  if  $n \bmod p = 0$ , otherwise  $\eta = 1$ . Notably,  $\ell_2$  should not be ignored here, as CPGP is an exact version (rather than an approximation) of PGP. On the one hand,  $\ell_2$  is needed to make  $\ell_1$  comparable among different sizes of  $p$ , as the sample size in  $\ell_1$  changes with  $p$ . On the other hand, dropping  $\ell_2$  may lead to worse performance, as illustrated in the following example, as well as the simulation study in Section 4 where an approximate CPGP is discussed.

**Example 1.** Consider the synthetic periodic signal in Fan et al. (2018) with data size  $n = 4,000$ , a sampling frequency  $f_s = 1$  Hz, and an SNR of  $-18$  dB; refer to Section 4 for details. We fit a classic PGP in Eq. (1) using the correlation function in Eq. (7) with parameters  $\theta = 15$ ,  $\delta = 3$  and  $d = 1$ . We show the waveforms of its full log-likelihood  $\ell$  and its first composite log-likelihood  $\ell_1$  changing with  $p$  in Fig. 1. It is seen that  $\ell_1$  fluctuates dramatically as  $p$  changes, because a changing signal length (i.e.,  $kp$ ) is used in  $\ell_1$ . In the bottom panel of Fig. 1, we further show the normalized  $\ell_1$  (i.e.,  $\ell_1/(kp)$ ), which still fluctuates considerably. The highest value of the full likelihood  $\ell$  locates at  $p = 200$  (i.e., the true period). Yet, the highest value of  $\ell_1$  or  $\ell_1/(kp)$  locates at a much larger  $p$ . Clearly, the second composite log-likelihood  $\ell_2$  should not be ignored here.

After the signal is divided into  $k$  segments  $\mathbf{y}_r$  ( $r = 1, 2, \dots, k$ ) and the remaining  $\mathbf{y}_*$ ,

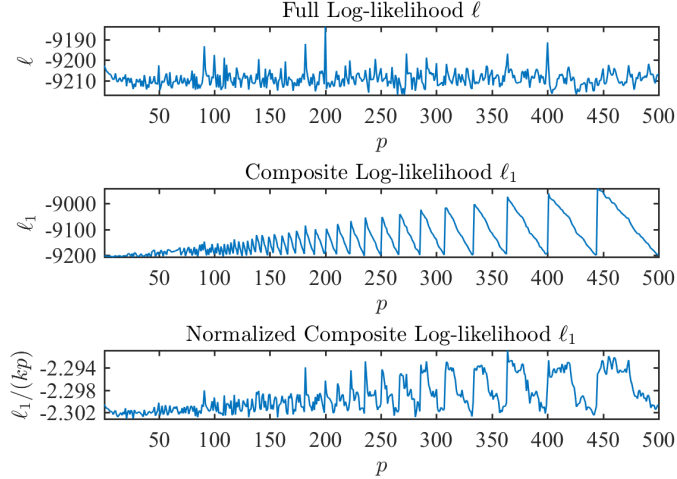


Figure 1: Values of  $\ell$  and  $\ell_1$  changing with  $p$ .

the covariance matrix between  $\mathbf{y}_r$  and  $\mathbf{y}_s$  is  $\sigma^2 (\mathbf{R} + \delta^2 \mathbf{I}_p)$  if  $r = s$ , and  $\sigma^2 \mathbf{R}$  if  $r \neq s$ , where

$$\mathbf{R} = \begin{bmatrix} \psi_\phi(t_1, t_1) & \cdots & \psi_\phi(t_1, t_p) \\ \vdots & \ddots & \vdots \\ \psi_\phi(t_p, t_1) & \cdots & \psi_\phi(t_p, t_p) \end{bmatrix};$$

the covariance matrix between  $\mathbf{y}_r$  and  $\mathbf{y}_*$  is  $\sigma^2 \mathbf{R}_\bullet$ , where

$$\mathbf{R}_\bullet = \begin{bmatrix} \psi_\phi(t_1, t_1) & \cdots & \psi_\phi(t_1, t_{n-kp}) \\ \vdots & \ddots & \vdots \\ \psi_\phi(t_p, t_1) & \cdots & \psi_\phi(t_p, t_{n-kp}) \end{bmatrix};$$

the covariance matrix for  $\mathbf{y}_*$  is  $\sigma^2 (\mathbf{R}_* + \delta^2 \mathbf{I}_{n-kp})$ , where

$$\mathbf{R}_* = \begin{bmatrix} \psi_\phi(t_1, t_1) & \cdots & \psi_\phi(t_1, t_{n-kp}) \\ \vdots & \ddots & \vdots \\ \psi_\phi(t_{n-kp}, t_1) & \cdots & \psi_\phi(t_{n-kp}, t_{n-kp}) \end{bmatrix}.$$

Next, we obtain a key result for the decomposition of correlation matrix  $\mathbf{K}$  and the

properties of matrices  $\mathbf{R}$  and  $\mathbf{R}_*$ .

**Proposition 1.** *The correlation matrix  $\mathbf{K}$  by Eq. (7) can be decomposed as*

$$\mathbf{K} = \begin{bmatrix} \mathbf{R} & \cdots & \mathbf{R} & \mathbf{R}_\bullet \\ \vdots & \ddots & \vdots & \vdots \\ \mathbf{R} & \cdots & \mathbf{R} & \mathbf{R}_\bullet \\ \mathbf{R}_\bullet^T & \cdots & \mathbf{R}_\bullet^T & \mathbf{R}_* \end{bmatrix}, \quad (9)$$

where  $\mathbf{R}$  is a symmetric circulant matrix and  $\mathbf{R}_*$  is a symmetric Toeplitz matrix.

The joint distribution of segments  $\mathbf{Y} = [\mathbf{y}_1^T, \dots, \mathbf{y}_k^T]^T$  is

$$\begin{aligned} \mathbf{Y} &\sim \mathcal{N}(\mathbf{\Gamma}\boldsymbol{\beta}, \sigma^2\boldsymbol{\Sigma}) \\ &\sim \mathcal{N}\left(\begin{bmatrix} \mathbf{\Gamma}_1\boldsymbol{\beta} \\ \vdots \\ \mathbf{\Gamma}_k\boldsymbol{\beta} \end{bmatrix}, \sigma^2 \begin{bmatrix} \mathbf{R} + \delta^2\mathbf{I}_p & \cdots & \mathbf{R} \\ \vdots & \ddots & \vdots \\ \mathbf{R} & \cdots & \mathbf{R} + \delta^2\mathbf{I}_p \end{bmatrix}\right), \end{aligned}$$

where  $\mathbf{\Gamma}_i = [\mathbf{f}(t_{1+(i-1)p}), \dots, \mathbf{f}(t_{ip})]^T$  for  $i = 1, \dots, k$ . Then, the first composite log-likelihood  $\ell_1$ , up to a constant, can be written as

$$\ell_1 = -\frac{1}{2} \left( \log |\sigma^2\boldsymbol{\Sigma}| + \frac{(\mathbf{Y} - \mathbf{\Gamma}\boldsymbol{\beta})^T \boldsymbol{\Sigma}^{-1} (\mathbf{Y} - \mathbf{\Gamma}\boldsymbol{\beta})}{\sigma^2} \right). \quad (10)$$

The distribution of  $\mathbf{y}_*$ , conditional on  $\mathbf{y}_1, \dots, \mathbf{y}_k$ , is  $\mathbf{y}_* | \mathbf{Y} \sim \mathcal{N}(\boldsymbol{\mu}, \sigma^2\boldsymbol{\Pi})$  with the mean  $\boldsymbol{\mu} = \mathbf{\Gamma}_*\boldsymbol{\beta} + \boldsymbol{\Xi}^T\boldsymbol{\Sigma}^{-1}(\mathbf{Y} - \mathbf{\Gamma}\boldsymbol{\beta})$  and the covariance matrix  $\boldsymbol{\Pi} = \mathbf{R}_* + \delta^2\mathbf{I}_{n-kp} - \boldsymbol{\Xi}^T\boldsymbol{\Sigma}^{-1}\boldsymbol{\Xi}$ , where  $\boldsymbol{\Xi} = [\mathbf{R}_\bullet^T \cdots \mathbf{R}_\bullet^T]^T$  and  $\mathbf{\Gamma}_* = [\mathbf{f}(t_{kp+1}), \dots, \mathbf{f}(t_n)]^T$ . Then, the second composite log-likelihood  $\ell_2$ , up to some constants, can be written as

$$\ell_2 = -\frac{1}{2} \left( \log |\sigma^2\boldsymbol{\Pi}| + \frac{(\mathbf{y}_\bullet - \mathbf{\Gamma}_*\boldsymbol{\beta})^T \boldsymbol{\Pi}^{-1} (\mathbf{y}_\bullet - \mathbf{\Gamma}_*\boldsymbol{\beta})}{\sigma^2} \right), \quad (11)$$

where  $\mathbf{y}_\bullet = \mathbf{y}_* - \mathbf{\Xi}^T \mathbf{\Sigma}^{-1} \mathbf{Y}$  and  $\mathbf{\Gamma}_\bullet = \mathbf{\Gamma}_* - \mathbf{\Xi}^T \mathbf{\Sigma}^{-1} \mathbf{\Gamma}$ . Note that if  $p > n$ , then the composite log-likelihood  $\ell_1$  reduces to zero, and the composite log-likelihood  $\ell_2$  reduces to  $\ell_2 = -1/2(\log |\sigma^2 \mathbf{R}_*| + (\mathbf{y}_* - \mathbf{\Gamma}_* \boldsymbol{\beta})^T \mathbf{R}_*^{-1} (\mathbf{y}_* - \mathbf{\Gamma}_* \boldsymbol{\beta}) / \sigma^2)$ .

### 3.2 Scalable Parameter Estimation

In accordance with Eqs. (10) and (11), the assessments of  $\ell_1$  and  $\ell_2$  require the determinant and inverse of  $\mathbf{\Sigma}$  and  $\mathbf{\Pi}$ , respectively. Since  $\mathbf{\Pi} = \mathbf{R}_* + \delta^2 \mathbf{I}_{n-kp} - \mathbf{\Xi}^T \mathbf{\Sigma}^{-1} \mathbf{\Xi}$ , the key challenge lies in the calculation of  $|\mathbf{\Sigma}|$  and  $\mathbf{\Sigma}^{-1}$ . In Proposition 2, we show that they can be substantially simplified by utilizing the matrix inversion lemma (Sherman and Morrison, 1950) and Sylvester determinant theorem (Akritas et al., 1996). The matrix inversion lemma is also known as the Woodbury, Sherman, and Morrison formula.

**Proposition 2.** *The inverse and determinant of  $\mathbf{\Sigma}$  can be simplified as*

$$\mathbf{\Sigma}^{-1} = \frac{k \mathbf{I}_{kp} - \mathbf{V} (\mathbf{I}_p - \mathbf{R}_\delta^{-1}) \mathbf{V}^T}{\delta^2 k}, \quad (12)$$

and

$$|\mathbf{\Sigma}| = \delta^{2kp} |\mathbf{R}_\delta|, \quad (13)$$

where  $\mathbf{R}_\delta = \mathbf{I}_p + k \mathbf{R} / \delta^2$  and  $\mathbf{V} = \begin{bmatrix} \mathbf{I}_p & \cdots & \mathbf{I}_p \end{bmatrix}^T$ .

According to Proposition 1, the matrix  $\mathbf{R}$  is a symmetric circulant matrix. Thus, the matrices  $\mathbf{R}_\delta$  and  $\mathbf{R}_\delta^{-1}$  in Proposition 2 are symmetric circulant matrices. Then, FFT method (Brigham, 1988) can be applied to compute  $\mathbf{R}_\delta^{-1}$  and  $|\mathbf{R}_\delta|$  with a computational complexity of  $\mathcal{O}(p \log p)$ . The MATLAB toolbox "smt" (Redivo-Zaglia and Rodriguez, 2012) can be used for implementation.

By plugging Eq. (12) into the formulas of  $\mathbf{y}_\bullet$ ,  $\mathbf{\Gamma}_\bullet$ , and  $\mathbf{\Pi}$  defined above, we have

$$\begin{cases} \mathbf{y}_\bullet &= \mathbf{y}_* - \frac{k}{\delta^2} \mathbf{R}_\bullet^T \mathbf{R}_\delta^{-1} \bar{\mathbf{y}} \\ \mathbf{\Gamma}_\bullet &= \mathbf{\Gamma}_* - \frac{k}{\delta^2} \mathbf{R}_\bullet^T \mathbf{R}_\delta^{-1} \bar{\mathbf{\Gamma}} \\ \mathbf{\Pi} &= \mathbf{R}_* + \delta^2 \mathbf{I}_{n-kp} - \frac{k}{\delta^2} \mathbf{R}_\bullet^T \mathbf{R}_\delta^{-1} \mathbf{R}_\bullet \end{cases},$$

where  $\bar{\mathbf{y}} = (\mathbf{y}_1 + \dots + \mathbf{y}_k) / k$  and  $\bar{\mathbf{\Gamma}} = (\mathbf{\Gamma}_1 + \dots + \mathbf{\Gamma}_k) / k$ . Here,  $\mathbf{R}^T \mathbf{R}_\delta^{-1} \mathbf{R}$  is a symmetric circulant matrix because the product of circulant matrices is still circulant. The matrix  $\mathbf{R}_\bullet^T \mathbf{R}_\delta^{-1} \mathbf{R}_\bullet$  (a sub-matrix of  $\mathbf{R}^T \mathbf{R}_\delta^{-1} \mathbf{R}$ ) is a symmetric Toeplitz matrix, and so is  $\mathbf{\Pi}$ . Then,  $\mathbf{\Pi}$  can be calculated in  $\mathcal{O}(p \log p)$  time because we only need to compute the first row/column of  $\mathbf{\Pi}$  via FFT. We can use the Cholesky factorization algorithm for semidefinite Toeplitz matrices (Stewart, 1997) to calculate  $\mathbf{\Pi}^{-1}$  and  $|\mathbf{\Pi}|$ , which requires  $\mathcal{O}((n - kp)^2)$  time. It is straightforward to show that this complexity is always smaller than  $\mathcal{O}(p^2)$ . Note that we may further accelerate the calculation of  $\mathbf{\Pi}^{-1}$  in  $\mathcal{O}(p \log p)$  time by embedding  $\mathbf{\Pi}$  into some circulant matrix, but the calculation of  $|\mathbf{\Pi}|$  cannot be further improved. Thus, the embedding circulant matrix method cannot further improve the complexity for calculating  $\ell_2$  (involving both  $\mathbf{\Pi}^{-1}$  and  $|\mathbf{\Pi}|$ ). Here, we consider only the Cholesky factorization algorithm.

By solving  $\partial \ell / \partial \boldsymbol{\beta} = 0$  and  $\partial \ell / \partial \sigma^2 = 0$ , we obtain the estimations of  $\boldsymbol{\beta}$  and  $\sigma^2$

$$\hat{\boldsymbol{\beta}} = (\mathbf{S}_{\Gamma\Gamma} + \eta \mathbf{\Gamma}_\bullet^T \mathbf{\Pi}^{-1} \mathbf{\Gamma}_\bullet)^{-1} (\mathbf{S}_{\Gamma Y} + \eta \mathbf{\Gamma}_\bullet^T \mathbf{\Pi}^{-1} \mathbf{y}_\bullet), \quad (14)$$

and

$$\hat{\sigma}^2 = \frac{(\mathbf{S}_{YY} + \eta \mathbf{y}_\bullet^T \mathbf{\Pi}^{-1} \mathbf{y}_\bullet) - \hat{\boldsymbol{\beta}}^T (\mathbf{S}_{\Gamma\Gamma} + \eta \mathbf{\Gamma}_\bullet^T \mathbf{\Pi}^{-1} \mathbf{\Gamma}_\bullet) \hat{\boldsymbol{\beta}}}{n}, \quad (15)$$

where

$$\begin{cases} \mathbf{S}_{\Gamma\Gamma} &= \mathbf{\Gamma}^T \mathbf{\Sigma}^{-1} \mathbf{\Gamma} = \frac{\mathbf{\Gamma}^T \mathbf{\Gamma} - k \bar{\mathbf{\Gamma}}^T \bar{\mathbf{\Gamma}} + k \bar{\mathbf{\Gamma}}^T \mathbf{R}_\delta^{-1} \bar{\mathbf{\Gamma}}}{\delta^2} \\ \mathbf{S}_{\Gamma\mathbf{Y}} &= \mathbf{\Gamma}^T \mathbf{\Sigma}^{-1} \mathbf{Y} = \frac{\mathbf{\Gamma}^T \mathbf{Y} - k \bar{\mathbf{\Gamma}}^T \bar{\mathbf{y}} + k \bar{\mathbf{\Gamma}}^T \mathbf{R}_\delta^{-1} \bar{\mathbf{y}}}{\delta^2} . \\ \mathbf{S}_{\mathbf{Y}\mathbf{Y}} &= \mathbf{Y}^T \mathbf{\Sigma}^{-1} \mathbf{Y} = \frac{\mathbf{Y}^T \mathbf{Y} - k \bar{\mathbf{y}}^T \bar{\mathbf{y}} + k \bar{\mathbf{y}}^T \mathbf{R}_\delta^{-1} \bar{\mathbf{y}}}{\delta^2} \end{cases}$$

Specifically, if  $\mathbf{\Gamma}_1 = \dots = \mathbf{\Gamma}_k$ ,  $\mathbf{S}_{\Gamma\Gamma} = k \bar{\mathbf{\Gamma}}^T \mathbf{R}_\delta^{-1} \bar{\mathbf{\Gamma}} / \delta^2$  and  $\mathbf{S}_{\Gamma\mathbf{Y}} = k \bar{\mathbf{\Gamma}}^T \mathbf{R}_\delta^{-1} \bar{\mathbf{y}} / \delta^2$ . Here, calculating  $\hat{\boldsymbol{\beta}}$  and  $\hat{\sigma}^2$  involves the calculation of  $\mathbf{R}_\delta^{-1}$  and  $\mathbf{\Pi}^{-1}$  whose dimensionalities are no more than  $p$ . This shows that the estimations of  $\hat{\boldsymbol{\beta}}$  and  $\hat{\sigma}^2$  are scalable.

By plugging Eqs. (13), (14), and (15) into Eqs. (10) and (11), the log-likelihood  $\ell(\theta, \delta, p, d)$  in Eq. (8) can be written as

$$\hat{\ell}(\theta, \delta, p, d) = -\frac{\log \hat{\sigma}^{2n} \delta^{2kp} + \log |\mathbf{R}_\delta| |\mathbf{\Pi}|^\eta + n}{2}. \quad (16)$$

Here, the evaluation of  $\hat{\ell}(\theta, \delta, p, d)$  involves calculating  $\mathbf{R}_\delta$  and  $\mathbf{\Pi}$ , which requires  $\mathcal{O}(p \log p)$  and  $\mathcal{O}(p^2)$  time, respectively. Thus, calculating the likelihoods of CPGP requires a computational complexity of  $\mathcal{O}(p^2)$  in general. When  $p$  divides  $n$  ( $\ell = \ell_1$  and  $\ell_2 = 0$ ), the evaluation of  $\hat{\ell}(\theta, \delta, p, d)$  involves calculating only  $\mathbf{\Sigma}^{-1}$  and  $|\mathbf{\Sigma}|$ . According to Proposition 2, such a special case requires only  $\mathcal{O}(p \log p)$  time. As a comparison, the PGP and TPGP have a complexity of  $\mathcal{O}(n^3)$  and  $\mathcal{O}(n^2)$ , respectively. Next, we give an example to illustrate the speeds of PGP, TPGP, and CPGP for calculating likelihoods.

**Example 2.** Consider the synthetic periodic signals in Example 1 with its length  $n$  ranging from 1,000 to 500,000. The PGP, TPGP, and CPGP models are implemented to evaluate the log-likelihood  $\hat{\ell}$  with parameters  $\theta = 15$  and  $\delta = 10$ . The average computing time of 100 trials is reported in Fig. 2. Unlike PGP and TPGP, the proposed CPGP has a computing time independent of the signal length. Moreover, CPGP is substantially faster than PGP and TPGP for long signals. In addition, we can see that CPGP with a predetermined period  $T = 100$  (i.e.,  $p = 100$  and  $d = 1$ ) is faster than that with  $T = 11$  (i.e.,  $p = 11$  and

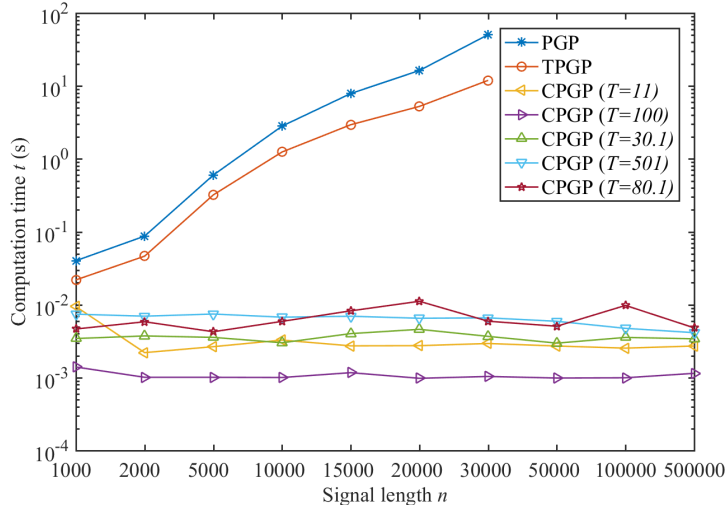


Figure 2: Average computational time of PGP, TPGP, and CPGP.

$d = 1$ ), because its complexity improves from  $\mathcal{O}(p^2)$  in general to  $\mathcal{O}(p \log p)$  when  $p$  divides  $n$ . CPGP can also handle decimal periods, as seen in the cases of  $T = 30.1$  ( $p = 301$  and  $d = 10$ ) and  $T = 80.1$  ( $p = 801$  and  $d = 10$ ).

In practice, the sampling frequency  $f_s$  for collecting data is usually specified in advance, while the period  $T = p/(df_s)$  is often unknown (and so is the segment length  $p$ ). There are often numerous local optimums in likelihoods with regard to  $p$ , as shown in Fig. 1, and thus estimating  $p$  is non-trivial. In this work, we propose to locate the maximum value of  $\hat{\ell}(\theta, \delta, p, d_*)$  in Eq. (16) by scanning  $p$  in  $\mathcal{I} = \{1, 2, \dots, d_* p_{max}\}$  before a search algorithm is applied to estimate  $\theta$  and  $\delta^2$ , where  $d_*$  is a tuning parameter such that  $1 \leq d_* \leq d$  for computational saving. That is, we will first locate the maximum log-likelihood  $\hat{\ell}_{\mathcal{I}}(\theta, \delta, d_*) = \max_{p \in \mathcal{I}} \hat{\ell}(\theta, \delta, p, d_*)$  by scanning  $p$  in  $\mathcal{I}$  and then optimize  $\hat{\ell}_{\mathcal{I}}(\theta, \delta, d_*)$  to estimate  $\theta$  and  $\delta^2$  via some searching algorithms, i.e.,

$$\hat{\theta}, \hat{\delta} = \text{maximize}_{\theta, \delta} \left\{ \hat{\ell}_{\mathcal{I}}(\theta, \delta, d_*) \right\}. \quad (17)$$

Many heuristic optimization algorithms, such as gradient descent algorithms, can be used here, and we adopt the Hooke-Jeeves searching algorithm implemented by the MATLAB

toolbox “dace” (Lophaven et al., 2002).

By plugging the optimized  $\hat{\theta}$  and  $\hat{\delta}$  from Eq. (17) into  $\hat{\ell}(\theta, \delta, p, d)$  in Eq. (16), we have (given  $p$  and  $d$ )

$$\hat{\ell}(\hat{\theta}, \hat{\delta}, p, d) = -\frac{\log \hat{\sigma}^{2n} \hat{\delta}^{2kp} + \log |\hat{\mathbf{R}}_{\hat{\delta}}| |\hat{\mathbf{\Pi}}|^\eta + n}{2}, \quad (18)$$

where  $\hat{\mathbf{R}}_{\hat{\delta}}$  and  $\hat{\mathbf{\Pi}}$  can be obtained by plugging  $\hat{\theta}$  and  $\hat{\delta}$  into  $\mathbf{R}_\delta$  and  $\mathbf{\Pi}$ . The waveform peak of  $\hat{\ell}(\hat{\theta}, \hat{\delta}, p, d)$  in Eq. (18) locates at the true period  $\hat{T} = \hat{p}/(df_s)$  and its multiples; see Fig. 1 for an example. Due to the existence of numerous local optimums, enumerating  $p$  in  $\mathcal{T}$  is needed for optimization, i.e.,

$$\hat{p} = \arg \max_{p \in \mathcal{T}} \left\{ \hat{\ell}(\hat{\theta}, \hat{\delta}, p, d) \right\}, \quad (19)$$

where  $\mathcal{T} = \{1, 2, \dots, dp_{max}\}$  is the searching range for  $p$ . Specifically,  $\mathcal{I} = \mathcal{T}$  if  $d = d_*$ . Please refer to Supplementary Materials for a detailed description and the pseudo codes for the proposed optimization of Eqs. (17) and (19). The enumerating step for  $p$  can be computed in a parallel or distributed manner to further reduce the computing time if applicable.

The settings of  $\mathcal{I}$  and  $\mathcal{T}$  depend on a balance between the desired estimation accuracy and the available computational budget. When the sampling frequency  $f_s$  is considerably high (that is, the number of points in one period is reasonably large, e.g., larger than 100), setting  $d = d_* = 1$  (i.e.,  $\mathcal{T} = \mathcal{I}$ ) suffices, which will lead to integer period estimates. Otherwise, we may set  $d > 1$  and  $d \geq d_* \geq 1$  to enable period estimates having decimal points. Empirical studies show that  $d = d_*$  is not always necessary, and  $d_* = 1$  suffices in all of our numerical studies. As the searching range of  $p$  will generally include more elements when dealing with decimal periods than integer periods, computing decimal periods would generally need more time, and thus some common choices suggested are  $d_* = 1, d = 5$  and  $d_* = 1, d = 10$ . The tuning parameter  $p_{max}$  in  $\mathcal{I}$  and  $\mathcal{T}$  is often chosen according

to the prior knowledge of the signal, such that  $p_{max}/f_s$  is at least greater than the true period. For example, as the fundamental frequency of voiced speeches ranges approximately from 80 Hz to 300 Hz, we should set  $p_{max}$  such that  $f_s/p_{max}$  is smaller than 80 Hz. In addition, we could guess the true period  $T$  (and hence  $p_{max}$ ) according to the waveform of the likelihood function with a gradual increase of  $p_{max}$ , until the likelihood exhibits approximately periodic local optimums.

It is worth to remark that computing the likelihoods of CPGP requires a computational complexity of  $\mathcal{O}(p^2)$  in general and  $\mathcal{O}(p \log p)$  when  $p$  divides  $n$ , while the total computational complexity of CPGP considering the estimation of period is  $\mathcal{O}(d^3 p_{max}^3)$ . As both  $p$  and  $p_{max}$  are independent of and much smaller than  $n$  in practice, CPGP remains scalable. In this work, we emphasize more on the complexity for calculating likelihoods, because we want to make a fair comparison between CPGP and current PGP-based models that assume known periods. Although the proposed period estimation in CPGP can be embedded into PGP, it is not applicable in practice, because the optimization in (19) often requires evaluating the likelihood function thousands of times where both the PGP and TPGP would be prohibitively slow.

### 3.3 Scalable Model Prediction

As shown by Jones et al. (1998), the BLUP of  $y(t)$  can be obtained by maximizing the joint likelihood  $y(t)$  and  $\mathbf{y}$  with regard to  $y(t)$ , that is,  $\hat{y}(t) = \arg \max_{y(t)} \Pr(y(t), \mathbf{y})$ . Similar to the likelihood decomposition in Section 3.1, the joint distribution  $\Pr(y(t), \mathbf{y})$  can be decomposed into two parts

$$\Pr(y(t), \mathbf{y}) = \Pr(y(t), \mathbf{y}_* | \mathcal{Y}) \Pr(\mathcal{Y}),$$

where  $\Pr(y(t), \mathbf{y}_* | \mathcal{Y})$  is the joint distribution of  $\{y(t), \mathbf{y}_*\}$  conditional on  $\mathcal{Y}$ . Thus, we have

$$\hat{y}(t) = \arg \max_{y(t)} \Pr(y(t), \mathbf{y}_* | \mathcal{Y}),$$

and  $\Pr(y(t), \mathbf{y}_* | \mathcal{Y})$  can be further written as

$$\begin{bmatrix} y(t) \\ \mathbf{y}_* \end{bmatrix} \sim \left( \begin{bmatrix} \mu(t) \\ \boldsymbol{\mu} \end{bmatrix}, \sigma^2 \begin{bmatrix} \pi(t) & \boldsymbol{\gamma}_\bullet^T(t) \\ \boldsymbol{\gamma}_\bullet(t) & \boldsymbol{\Pi} \end{bmatrix} \right),$$

where

$$\begin{cases} \mu(t) &= \mathbf{f}^T(t) \boldsymbol{\beta} + \boldsymbol{\gamma}^T(t) \boldsymbol{\Sigma}^{-1} (\mathcal{Y} - \boldsymbol{\Gamma}) \\ \pi(t) &= 1 + \delta^2 - \boldsymbol{\gamma}^T(t) \boldsymbol{\Sigma}^{-1} \boldsymbol{\gamma}(t) \\ \boldsymbol{\gamma}_\bullet(t) &= \boldsymbol{\gamma}_*(t) - \boldsymbol{\Xi}^T \boldsymbol{\Sigma}^{-1} \boldsymbol{\gamma}(t) \end{cases}. \quad (20)$$

Here,  $\boldsymbol{\gamma}(t)$  and  $\boldsymbol{\gamma}_*(t)$  represent the correlation between  $y(t)$  and  $\mathcal{Y}$  and the correlation between  $y(t)$  and  $\mathbf{y}_*$ , respectively. Therefore, given  $\boldsymbol{\beta}$ ,  $\sigma$ ,  $\theta$ ,  $\delta$ , and  $p$ , we have the prediction  $\hat{y}(t) = \mu(t) + \boldsymbol{\gamma}_\bullet^T(t) \boldsymbol{\Pi}^{-1} (\mathbf{y}_* - \boldsymbol{\mu})$  and its variance  $\text{Var}(\hat{y}(t)) = \sigma^2 (\pi(t) - \boldsymbol{\gamma}_\bullet^T(t) \boldsymbol{\Pi}^{-1} \boldsymbol{\gamma}_\bullet(t))$ .

With Eq. (12) plugged in, Eq. (20) can be simplified as

$$\begin{cases} \mu(t) &= \mathbf{f}^T(t) \boldsymbol{\beta} + \frac{k}{\delta^2} \bar{\boldsymbol{\gamma}}^T(t) \mathbf{R}_\delta^{-1} (\bar{\mathbf{y}} - \bar{\boldsymbol{\Gamma}} \boldsymbol{\beta}) \\ \pi(t) &= 1 + \delta^2 - \frac{k}{\delta^2} \bar{\boldsymbol{\gamma}}^T(t) \mathbf{R}_\delta^{-1} \bar{\boldsymbol{\gamma}}(t) \\ \boldsymbol{\gamma}_\bullet(t) &= \boldsymbol{\gamma}_*(t) - \frac{k}{\delta^2} \mathbf{R}_\bullet^T \mathbf{R}_\delta^{-1} \bar{\boldsymbol{\gamma}}(t) \end{cases},$$

where  $\bar{\boldsymbol{\gamma}}(t)$  denotes the correlation between  $y(t)$  and  $\mathbf{y}_1$ . Then, by substituting  $\boldsymbol{\beta}$  with  $\hat{\boldsymbol{\beta}}$ , we can obtain a computationally efficient formula of BLUP

$$\begin{aligned} \hat{y}(t) &= \mathbf{f}^T(t) \hat{\boldsymbol{\beta}} + \frac{k}{\delta^2} \bar{\boldsymbol{\gamma}}^T(t) \mathbf{R}_\delta^{-1} (\bar{\mathbf{y}} - \bar{\boldsymbol{\Gamma}} \hat{\boldsymbol{\beta}}) \\ &\quad + \boldsymbol{\gamma}_\bullet^T(t) \boldsymbol{\Pi}^{-1} (\mathbf{y}_\bullet - \boldsymbol{\Gamma}_\bullet \hat{\boldsymbol{\beta}}). \end{aligned} \quad (21)$$

Eq. (14) implies that  $\text{Var}(\hat{\boldsymbol{\beta}}) = \sigma^2 (\mathbf{S}_{\Gamma\Gamma} + \eta \mathbf{\Gamma}_{\bullet}^T \mathbf{\Pi}^{-1} \mathbf{\Gamma}_{\bullet})^{-1}$ , and thus the variance of  $\hat{y}(t)$ , taking  $\hat{\boldsymbol{\beta}}$  into account, is

$$\begin{aligned} \text{Var}(\hat{y}(t)) &= \sigma^2 (\pi(t) - \boldsymbol{\gamma}_{\bullet}^T(t) \mathbf{\Pi}^{-1} \boldsymbol{\gamma}_{\bullet}(t)) \\ &\quad + \sigma^2 \boldsymbol{\omega}^T (\mathbf{S}_{\Gamma\Gamma} + \eta \mathbf{\Gamma}_{\bullet}^T \mathbf{\Pi}^{-1} \mathbf{\Gamma}_{\bullet})^{-1} \boldsymbol{\omega}, \end{aligned}$$

where  $\boldsymbol{\omega} = \mathbf{f}(t) - \frac{k}{\delta^2} \bar{\mathbf{\Gamma}}^T \mathbf{R}_{\delta}^{-1} \bar{\boldsymbol{\gamma}}(t) - \mathbf{\Gamma}_{\bullet}^T \mathbf{\Pi}^{-1} \boldsymbol{\gamma}_{\bullet}(t)$ .

Similar to the above, the MATLAB toolbox "smt" for circulant matrices (Redivo-Zaglia and Rodriguez, 2012) and the Cholesky factorization algorithm for semidefinite Toeplitz matrices (Stewart, 1997) can be applied to calculate this BLUP, which has a computational complexity of  $\mathcal{O}(p^2)$ .

## 4 Simulation Study

The PGP framework is mostly used in applications for periodicity detection. Here, we conduct a popular simulation for periodicity detection to evaluate the effectiveness of the proposed CPGP. We compare it with some state-of-the-art methods, including TPGP (Zhang et al., 2005), FNLS (Nielsen et al., 2017), NRC (Li et al., 2021), and MLPE (Wise et al., 1976). For a fair comparison, the proposed optimization provided in Eqs. (17) and (19) is also applied in TPGP to enable period estimation.

In addition, we also consider a variant of CPGP here, called the approximate CPGP (ACPGP), in order to study the importance of  $\ell_2$  in (8). The likelihood of ACPGP only includes the normalized  $\ell_1$ , i.e.,

$$\ell(\theta, \delta, p, d) = \frac{1}{kp} \ell_1. \quad (22)$$

In ACPGP, the MLE of  $\boldsymbol{\beta}$  and  $\sigma^2$  is  $\hat{\boldsymbol{\beta}} = \mathbf{S}_{\Gamma\Gamma}^{-1} \mathbf{S}_{\Gamma\mathbf{Y}}$  and  $\hat{\sigma}^2 = \frac{1}{n} (\mathbf{S}_{\mathbf{Y}\mathbf{Y}} - \hat{\boldsymbol{\beta}}^T \mathbf{S}_{\Gamma\Gamma} \hat{\boldsymbol{\beta}})$ , respec-

tively. Similar to Eq. (18), we have  $\hat{\ell}(\hat{\theta}, \hat{\delta}, p, d) = -\frac{1}{2kp} \left( \log \hat{\sigma}^{2kp} \hat{\delta}^{2kp} + \log |\hat{\mathbf{R}}_{\hat{\delta}}| + kp \right)$ , and the same optimization algorithm in Eqs. (17) and (19) can be used for parameter estimation. Notably, computing the likelihood of ACPGP requires  $\mathcal{O}(p \log p)$  time, which is generally faster than CPGP at the price of sacrificing certain accuracy.

Consider a widely discussed simulation on the synthetic signals in Fan et al. (2018), which are the periodic transients generated from the following equation:

$$x(t) = \sum_{i=0}^{\lfloor \frac{l}{T_0} \rfloor} e^{\frac{-\zeta 2\pi\omega(t-iT_0)^2}{\sqrt{1-\zeta^2}}} \sin 2\pi\omega(t-iT_0), \quad (23)$$

where  $\zeta = 0.01$  is the damping ratio,  $\omega = 0.055$  Hz is the natural frequency, the period is  $T_0 = 200$  seconds, and  $l$  is the time length of the signals. The signals  $x(t)$  are collected with a sampling frequency of  $f_s = 1$  Hz, and thus there are 200 signal points in one period. The contaminated signal  $y(t)$  (i.e., the simulated data) is generated by adding Gaussian white noises to the periodic signal  $x(t)$ . The focus here is periodicity detection.

In CPGP and ACPGP, as there are 200 points in one period, the searching range of  $p$  is set to  $[1, 500]$ , that is,  $\mathcal{I} = \mathcal{T} = \{1, 2, \dots, 500\}$ ,  $p_{max} = 500$  and  $d_* = d = 1$ . The searching range for the parameters  $\delta$  and  $\theta$  is set to  $[2, 20]$  and  $[1, 30]$ , respectively. Their initial values in the optimization algorithm are assigned to those that have the maximum value of  $\hat{\ell}_{\mathcal{I}}(\theta, \delta, d_*)$  among nine grid candidates in the two-dimensional searching space  $[2, 20] \times [1, 30]$ . Using the best initial values from a simple grid search would make CPGP more robust, especially when prior information (domain knowledge) is unavailable, as the likelihood may have many misleading local optimums. Throughout this paper, we use  $\mathbf{f}(t) = 1$  in CPGP for simplicity. In this study, both CPGP and TPGP use the same initial parameter settings, and thus they result in the same parameter estimations. Their difference lies in the computing time, where CPGP is much faster than TPGP. In FNLS, the max harmonic number is set to  $L = 30$ . We replicate the analysis 100 times where the signals are independently and randomly generated.

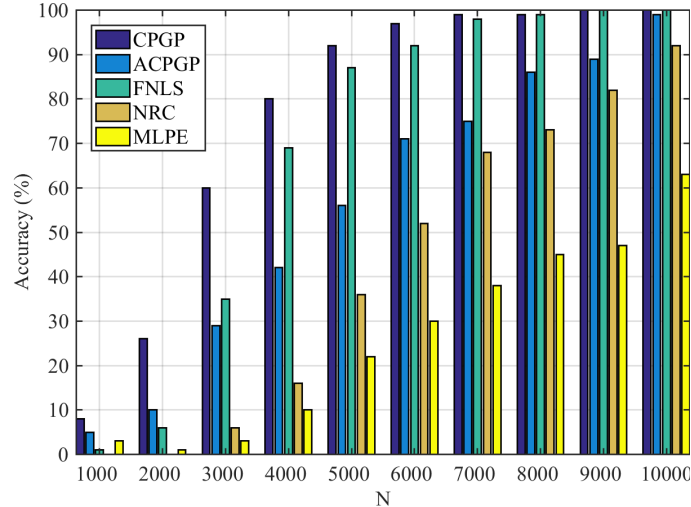


Figure 3: Period estimation accuracy of CPGP, ACPGP, FNLS, NRC, and MLPE changing with the signal length in the simulation study.

In Fig. 3, we show the period estimation accuracy (i.e., the probability of  $\hat{T} = T_0$  out of the 100 trials) of each method handling various signal lengths (from 1000 to 10000), where the SNR is  $-21$  dB. In Fig. 4, we show the period estimation accuracy of each method handling signals with various SNRs (from  $-25$  dB to  $-11$  dB), where the signal length is 5000. Notably, as TPGP has the same period estimates as CPGP, we do not show its results in these figures. Their difference lies in the computing time which is shown in Tab. 1.

In Figs. 3 and 4, compared with CPGP, ACPGP reports a lower period estimation accuracy in all cases, which suggests that the second composite likelihood  $\ell_2$  in (8) may play an important role here. It is seen that ACPGP only works reasonably well for long signals and increased SNR, but works badly for other cases. In practice, we only promote the use of CPGP for period detection due to its high accuracy and robustness. If we know in advance that the signal length will be very long and SNR will be high enough, ACPGP can be used considering its faster speed.

Additionally, it is seen from Fig. 3 that CPGP has substantially higher accuracy than FNLS, NRC, and MLPE for all signal lengths. As the signal length increases, all methods would eventually reach 100% accuracy, while CPGP converges considerably faster. Clearly,

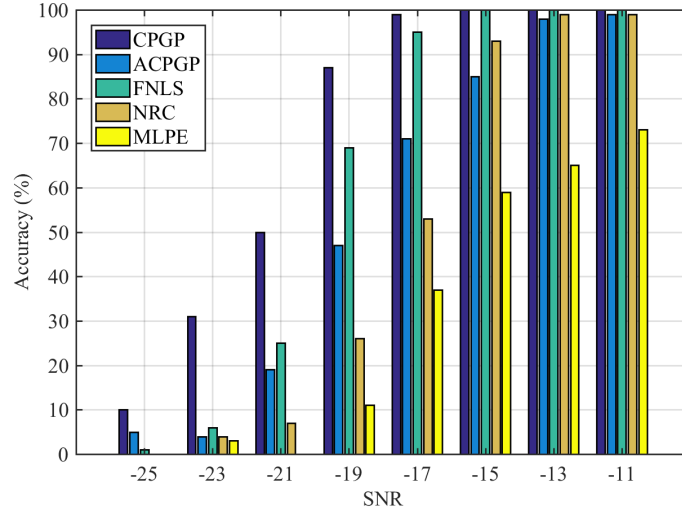


Figure 4: Period estimation accuracy of CPGP, ACPGP, FNLS, NRC, and MLPE changing with SNR in the simulation study.

CPGP outperforms its competitors and is able to accurately detect periodicity at an early stage. In addition, from Fig. 4, we can see that CPGP has substantially higher accuracy than other methods when the SNR is low, and all methods would have higher accuracy as the SNR increases. Above all, CPGP can process lower SNR signals more effectively via using fewer signal points compared with FNLS, NRC, and MLPE.

Notably, NRC and MLPE provide lower accuracy mainly because they do not consider the within-period correlations, which are meticulously modeled by CPGP. Different from FNLS that uses a number of Fourier bases to approximate the true signals, CPGP uses a non-parametric way to represent the signals where the roughness parameter  $\theta$  is optimized to adaptively model the within-period correlations. As shown in Fig. 5, the correlation function of PGP (and CPGP) is more flexible than that of FNLS. Most correlations in FNLS are quite small, and diagonal elements dominate the off-diagonal ones in the correlation matrix. Most of these off-diagonal correlation elements are negative, especially when  $L$  is large. Yet, it should be more reasonable and flexible to assume a zero (or near zero) correlation for two distant points. In addition, the position of these negative elements in the covariance matrix of FNLS is fixed given the tuning parameter  $L$  (although  $L$  can be

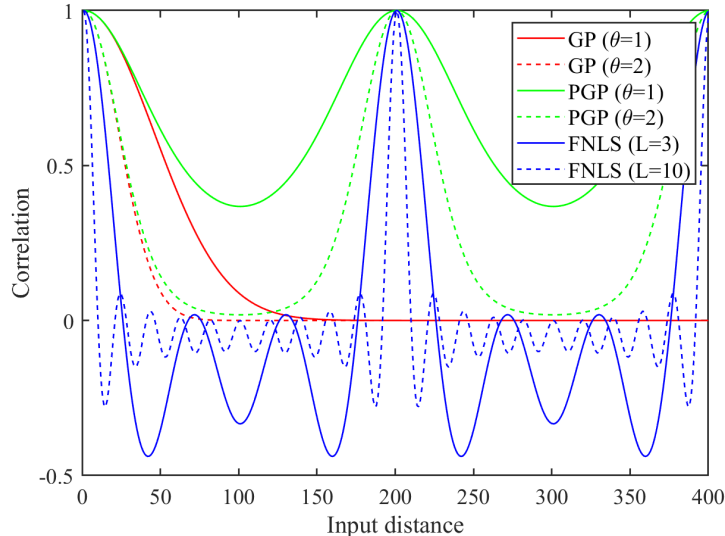


Figure 5: Correlation function of GP, PGP (CPGP), and FNLS

optimized via model selection criteria). Clearly, such a correlation structure in FNLS may not effectively utilize the spatial or temporal correlations of periodic data. The superior performance of CPGP is mainly due to its capability to model the circulant within-period correlations of periodic data.

In Tab. 1, we report the average computing time of 100 trials for each method dealing with various signal lengths. Here, TPGP is the slowest, and it may require several hours for modeling signals with only moderate lengths (e.g.  $n = 5000$ ). Notably, TPGP is much faster than the classic PGP model, and similarly fast compared to other PGP-based methods using approximation approaches discussed in Section 2. In contrast, the proposed CPGP is significantly faster than TPGP, which only requires around 18 seconds even for very long signals. As seen in Tab. 1, the computing time of CPGP and ACPGP does not increase along with the signal length, which indicates that the computational complexities of CPGP and ACPGP are scalable. ACPGP is faster but less accurate compared to CPGP.

In Tab. 1, although FNLS consumes less time than CPGP for short signals, it requires more time for long signals (e.g.,  $n \geq 10,000$ ). This is because its computational complexity is  $\mathcal{O}(nL)$  which grows with the signal length. Compared to CPGP and FNLS, NRC and

Table 1: Average computing time of 100 trials (unit: second).

$n$	TPGP	CPGP	ACPGP	FNLS	NRC	MLPE
1000	189.91	18.744	5.9217	0.6314	0.0117	0.0198
2000	897.01	18.960	5.6760	1.6991	0.0113	0.0216
3000	1771.5	18.809	5.7584	3.6112	0.0139	0.0247
4000	3167.2	19.308	6.0763	5.6430	0.0177	0.0304
5000	4899.6	19.634	5.9567	7.6847	0.0199	0.0328
6000	6129.8	18.307	5.9955	10.418	0.0216	0.0343
7000	8324.0	18.056	5.9258	11.620	0.0239	0.0359
8000	10878	18.172	6.0060	14.971	0.0265	0.0399
9000	13848	17.935	6.0506	15.912	0.0313	0.0453
10000	17076	18.337	6.1132	20.098	0.0341	0.0488

MLPE are faster but much less accurate (as shown in Figs. 3 and 4), since they ignore within-period correlations.

## 5 Real Case Study

### 5.1 Bearing Fault Detection

As one of the core components in rotating machinery, the rolling bearing directly affects the product quality and reliability of the rotating machines. However, bearings are prone to failure under complex working conditions, thus triggering periodic vibrations. A common solution to bearing fault detection is to apply period estimation methods to extract the fault period from the vibration signals. Accurate methods are needed to identify the fault period as early as possible because the complicated background noise may mask the periodic signals of the faulty bearing.

In this case study, the vibration data are downloaded from the Case Western Reserve University (CWRU) <sup>2</sup>. The type of bearings used is 6205-2RS JEM SKF, and the parameters of the test bearing are listed in Tab. 2. The bearing fault is set in the outer race, and the signals are collected from the testing rig with a sampling frequency of 48 kHz. According

<sup>2</sup><https://engineering.case.edu/bearingdatacenter/>

Table 2: Parameters of test bearing 6205-2RS JEM SKF

Type	6205-2RS JEM SKF
No. of rolling elements	9
Inside diameter (in)	0.9843
Outside diameter (in)	2.0472
Thickness (in)	0.5906
Ball diameter (in)	0.3126
Pitch diameter (in)	1.537
Approx. motor speed (rpm)	1747
Size of fault (mm)	0.021
Approx. fault frequency (Hz)	104
Approx. fault period (ms)	9.6

to Tab. 2, the fault characteristic frequency is 104 Hz, and the fault period is  $T_0 = 461$ .

The vibration signals have 100,000 sample points. The fault characteristic frequency cannot be directly located through conventional spectrum methods due to the complex background noise. Thus, we seek to detect the bearing fault from the time domain. The proposed CPGP method is applied to estimate the fault period from the vibration signals. As the sampling frequency is considerably high, the searching range for  $p$  is set to  $[1, 500]$ , that is,  $\mathcal{T} = \mathcal{I} = \{1, 2, \dots, 1,000\}$ ,  $p_{max} = 1,000$  and  $d = d_* = 1$ . The searching range for parameters  $\delta$  and  $\theta$  in CPGP is set to  $[0.01, 5]$  and  $[15, 20]$ , respectively. The initial values of  $\delta$  and  $\theta$  are obtained in a similar way to that in Section 4. To perform a comparison, NRC, MLPE, and FNLS are applied to estimate the fault period. The max harmonic number for FNLS is set to  $L = 30$ . To measure the accuracy of each method, a segment of signals is randomly drawn from the entire vibration signals with the signal length  $n$  ranging from 2,000 to 20,000. Following Li et al. (2021), the probability that the estimated period falls into  $\{0.95T_0, 1.05T_0\}$  is recorded as the detection accuracy. The experiment is repeated 100 times for each  $n$  ranging from 2,000 to 20,000, and we show their fault detection accuracy in Fig. 6.

Fig. 6 shows that the proposed CPGP performs substantially better than other methods, especially when the signal length is short (smaller than 6,000), which indicates that it

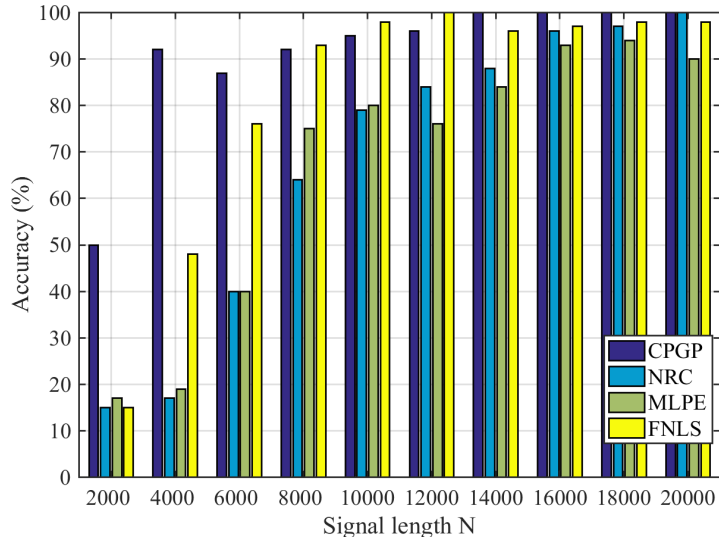


Figure 6: Period estimation accuracy of CPGP, NRC, MLPE, and FNLS on bearing vibration signals.

can be used to detect the bearing fault at an early stage. Compared with the accuracy of NRC and MLPE, the accuracy of CPGP is substantially higher, and it converges to 100% much faster as the signal length increases (longer than 14,000). Although the FNLS slightly outperforms CPGP when the signal length is moderate, its accuracy cannot converge to 100% even when the signals are sufficiently long. This is mainly because the real vibration signals are not strictly periodic and subject to significant noises. The steady convergence of CPGP indicates that it can perform robustly on real signals.

## 5.2 Pitch Estimation

Pitch estimation, which is also known as fundamental frequency estimation, is an intriguing research topic in the audio signal processing area (Nielsen et al., 2017). Researchers aim to produce a sequence of frequency values corresponding to the pitch of speech or musical recordings. Given a recording of monophonic music or speech, its pitch could be easily identified by humans. However, completing such a task is still challenging for AI because the signals usually comprise complex signal components and environment noises. The pitch can be estimated by the autocorrelation-based methods (e.g., NRC) or the likelihood-based

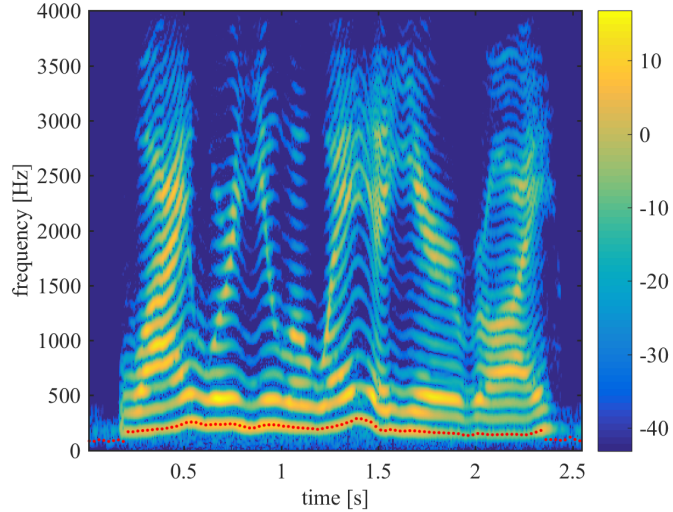


Figure 7: Estimated fundamental frequencies and spectrograms of the speech signals.

methods (e.g., MLPE). Yet, NRC and MLPE do not consider within-period correlations. A more complex method that can take within-period correlations into consideration is needed. In this case study, CPGP is applied to estimate the pitch of a voice speech recording and a monophonic music recording produced by the viola.

The signals are divided into short signal subsets ( $n = 200$  for the speech signals and  $n = 240$  for the music signals), and each subset is analyzed separately to display the flow of changing fundamental frequencies. The searching grids for  $p$  are  $\mathcal{I} = \{2, 3, \dots, 120\}$  and  $\mathcal{T} = \{2, 3, \dots, 600\}$  via setting  $d_* = 1$ ,  $d = 5$  and  $p_{max} = 120$ , because the sampling frequencies (8000 Hz) of these signals are relatively low. As the waveform of audio signals is considerably smoother and the strength of noises is weak, the searching range for parameters  $\delta$  and  $\theta$  in CPGP is set to  $[0.3, 0.5]$  and  $[2, 3]$ , respectively. We find that using the domain knowledge to specify searching ranges would help improve the performance.

As shown in Figs. 7 and 8, the estimated fundamental frequencies for both signals are marked as red spots on the spectrograms (Mitra and Kuo, 2006). The red spots match well with the patterns illustrated in the spectrograms, which indicates that CPGP can accurately estimate the period of audio and monophonic musical signals. This case study

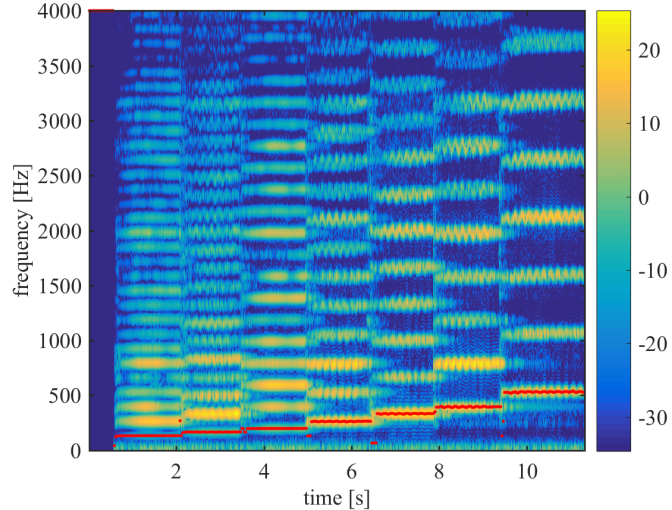


Figure 8: Estimated fundamental frequencies and spectrograms of the musical signals.

implies the great potential of applying CPGP in pitch estimation and melody extraction for audio and musical signals.

## 6 Conclusion

In this paper, a scalable modeling approach called CPGP is proposed to accelerate the parameter estimation and model prediction of PGP, thereby greatly substantiating its applicability for handling large-scale and low SNR periodic data. When periodic data are collected at grids, computing the likelihoods of CPGP only requires a computational complexity of  $\mathcal{O}(p^2)$  in general, and  $\mathcal{O}(p \log p)$  if  $p$  divides  $n$ ; its total computational complexity considering the estimation of periods is  $\mathcal{O}(d^3 p_{max}^3)$ , where the segment lengths  $p$  and  $p_{max}$  are independent of and much smaller than the data size  $n$  in practice. Different from conventional approximation approaches, CPGP has exactly the same likelihoods and thus maintains the same accuracy as PGP. The superior performances of CPGP in the simulations and case studies validates its usefulness in real-world applications.

An interesting future topic is how to further accelerate CPGP with desirable accuracy. In the simulation study, it is seen that the variant ACPGP runs faster than CPGP, but

its performance is not satisfactory. Simply sacrificing the second composite log-likelihood  $\ell_2$  to improve the speed is not a good idea. An alternative approach is to apply zero-padding of the data such that  $n$  can divide  $p$ , which will accelerate the computational complexity of evaluating likelihoods to  $\mathcal{O}(p \log p)$ . Yet, a straightforward application of zero-padding does not perform well in practice, especially when signals have non-constant trends. A meticulously designed zero-padding method with solid theoretical supports will be explored in our future works, which uses the circulant embedding method (Wood and Chan, 1994; Davies and Bryant, 2013) and the circulant approximation for the Toeplitz matrix.

The proposed CPGP assumes the data are strictly periodic, although it has been successfully applied to real applications in which signals are probably pseudo-periodic. A new efficient modeling approach may be required for pseudo-periodic signals with strong stretched or distorted variations of a repeating cycle. Another restrictive assumption is the noises are white Gaussian. These assumptions may limit the applications of the proposed CPGP. We will explore some extensions of CPGP to pseudo-periodic data contaminated with colored noises in future research.

## Supplementary Materials

The supplementary materials contain technical proofs of the theoretical results, details (including pseudo codes) of the proposed optimization for parameter estimation, and codes for reproducing all figures and tables in this article.

## Acknowledgments

We would like to thank the Editor (Robert B. Gramacy), an AE, and two referees for their valuable comments.

## Disclosure Statement

The authors report that there are no competing interests to declare.

## Funding

This work was supported in part by the National Natural Science Foundation of China under Grant 72101147 and in part by the Shanghai Pujiang Program under Grant 21PJ1405500.

## References

- Akritas, A. G., Akritas, E. K., and Malaschonok, G. I. (1996), “Various proofs of Sylvester’s (determinant) identity,” *Mathematics and Computers in Simulation*, 42, 585–593.
- Bevilacqua, M., Fassò, A., Gaetan, C., Porcu, E., and Velandia, D. (2016), “Covariance tapering for multivariate Gaussian random fields estimation,” *Statistical Methods & Applications*, 25, 21–37.
- Brigham, E. O. (1988), *The fast Fourier transform and its applications*, Prentice-Hall, Inc.
- Caragea, P. C. and Smith, R. L. (2007), “Asymptotic properties of computationally efficient alternative estimators for a class of multivariate normal models,” *Journal of Multivariate Analysis*, 98, 1417–1440.
- Chandola, V. and Vatsavai, R. R. (2011), “A gaussian process based online change detection algorithm for monitoring periodic time series,” in *Proceedings of the 2011 SIAM international conference on data mining*, SIAM, pp. 95–106.

- Choudhury, A., Nair, P. B., and Keane, A. J. (2002), “A data parallel approach for large-scale Gaussian process modeling,” in *Proceedings of the 2002 SIAM International Conference on Data Mining*, SIAM, pp. 95–111.
- Coeurjolly, J.-F. and Porcu, E. (2018), “Fast and exact simulation of complex-valued stationary Gaussian processes through embedding circulant matrix,” *Journal of Computational and Graphical Statistics*, 27, 278–290.
- Cressie, N. and Johannesson, G. (2008), “Fixed rank kriging for very large spatial data sets,” *Journal of the Royal Statistical Society: Series B (Statistical Methodology)*, 70, 209–226.
- Davies, T. M. and Bryant, D. (2013), “On circulant embedding for Gaussian random fields in  $\mathbb{R}^d$ ,” *Journal of Statistical Software*, 55, 1–21.
- Dietrich, C. R. and Newsam, G. N. (1997), “Fast and exact simulation of stationary Gaussian processes through circulant embedding of the covariance matrix,” *SIAM Journal on Scientific Computing*, 18, 1088–1107.
- Diggle, P. J., Moraga, P., Rowlingson, B., and Taylor, B. M. (2013), “Spatial and spatio-temporal log-Gaussian Cox processes: extending the geostatistical paradigm,” *Statistical Science*, 28, 542–563.
- Durrande, N., Hensman, J., Rattray, M., and Lawrence, N. D. (2016), “Detecting periodicities with Gaussian processes,” *PeerJ Computer Science*, 2, e50.
- Eidsvik, J., Shaby, B. A., Reich, B. J., Wheeler, M., and Niemi, J. (2014), “Estimation and prediction in spatial models with block composite likelihoods,” *Journal of Computational and Graphical Statistics*, 23, 295–315.
- Fan, W., Li, Y., Tsui, K. L., and Zhou, Q. (2018), “A noise resistant correlation method for

- period detection of noisy signals,” *IEEE Transactions on Signal Processing*, 66, 2700–2710.
- Fang, K. T., Li, R., and Sudjianto, A. (2006), *Design and modeling for computer experiments*, Chapman & Hall/CRC Computer Science & Data Analysis Series.
- Finley, A. O., Banerjee, S., Waldmann, P., and Ericsson, T. (2009), “Hierarchical spatial modeling of additive and dominance genetic variance for large spatial trial datasets,” *Biometrics*, 65, 441–451.
- Gramacy, R. B. (2020), *Surrogates: Gaussian process modeling, design, and optimization for the applied sciences*, Chapman and Hall/CRC.
- Guérin, J., de Paula Canuto, A. M., and Goncalves, L. M. G. (2020), “Robust Detection of Objects under Periodic Motion with Gaussian Process Filtering,” in *2020 19th IEEE International Conference on Machine Learning and Applications (ICMLA)*, IEEE, pp. 685–692.
- HajiGhassemi, N. and Deisenroth, M. (2014), “Analytic long-term forecasting with periodic Gaussian processes,” in *Artificial Intelligence and Statistics*, PMLR, pp. 303–311.
- Heagerty, P. J. and Lele, S. R. (1998), “A composite likelihood approach to binary spatial data,” *Journal of the American Statistical Association*, 93, 1099–1111.
- Jones, D. R., Schonlau, M., and Welch, W. J. (1998), “Efficient global optimization of expensive black-box functions,” *Journal of Global Optimization*, 13, 455–492.
- Katzfuss, M. and Guinness, J. (2021), “A general framework for Vecchia approximations of Gaussian processes,” *Statistical Science*, 36, 124–141.
- Kaufman, C. G., Schervish, M. J., and Nychka, D. W. (2008), “Covariance tapering for likelihood-based estimation in large spatial data sets,” *Journal of the American Statistical Association*, 103, 1545–1555.

- Klenske, E. D., Zeilinger, M. N., Schölkopf, B., and Hennig, P. (2015), “Gaussian process-based predictive control for periodic error correction,” *IEEE Transactions on Control Systems Technology*, 24, 110–121.
- Koulali, A. and Clarke, P. (2021), “Modelling quasi-periodic signals in geodetic time-series using Gaussian processes,” *Geophysical Journal International*, 226, 1705–1714.
- Li, Y., Zhao, H., Fan, W., and Shen, C. (2021), “Extended Noise Resistant Correlation Method for Period Estimation of Pseudoperiodic Signals,” *IEEE Transactions on Instrumentation and Measurement*, 70, 1–11.
- Li, Y. and Zhou, Q. (2016), “Pairwise meta-modeling of multivariate output computer models using nonseparable covariance function,” *Technometrics*, 58, 483–494.
- Lophaven, S. N., Nielsen, H. B., and Søndergaard, J. (2002), *Aspects of the matlab toolbox DACE*, Citeseer.
- MacKay, D. J. (1998), “Introduction to Gaussian processes,” *NATO ASI Series F Computer and Systems Sciences*, 168, 133–166.
- Mitra, S. K. and Kuo, Y. (2006), *Digital signal processing: a computer-based approach*, vol. 2, McGraw-Hill New York.
- Nielsen, J. K., Jensen, T. L., Jensen, J. R., Christensen, M. G., and Jensen, S. H. (2017), “Fast fundamental frequency estimation: Making a statistically efficient estimator computationally efficient,” *Signal Processing*, 135, 188–197.
- Park, C., Huang, J. Z., and Ding, Y. (2011), “Domain decomposition approach for fast Gaussian process regression of large spatial data sets,” *Journal of Machine Learning Research*, 12, 1697–1728.
- Quinn, B. and Thomson, P. (1991), “Estimating the frequency of a periodic function,” *Biometrika*, 78, 65–74.

- Quinonero-Candela, J. and Rasmussen, C. E. (2005), “A unifying view of sparse approximate Gaussian process regression,” *The Journal of Machine Learning Research*, 6, 1939–1959.
- Rasmussen, C. E. and Williams, C. K. I. (2006), “Gaussian Processes for Machine Learning,” *the MIT Press*.
- Redivo-Zaglia, M. and Rodriguez, G. (2012), “smt: a Matlab toolbox for structured matrices,” *Numerical Algorithms*, 59, 639–659.
- Sacks, J., Schiller, S. B., and Welch, W. J. (1989), “Designs for computer experiments,” *Technometrics*, 31, 41–47.
- Sang, H. and Huang, J. Z. (2012), “A full scale approximation of covariance functions for large spatial data sets,” *Journal of the Royal Statistical Society: Series B (Statistical Methodology)*, 74, 111–132.
- Santner, T. J., Williams, B. J., and Notz, W. I. (2013), *The design and analysis of computer experiments*, Springer Science & Business Media.
- Sherman, J. and Morrison, W. J. (1950), “Adjustment of an inverse matrix corresponding to a change in one element of a given matrix,” *The Annals of Mathematical Statistics*, 21, 124–127.
- Snelson, E. and Ghahramani, Z. (2007), “Local and global sparse Gaussian process approximations,” in *Artificial Intelligence and Statistics*, PMLR, pp. 524–531.
- Stein, M. L. (2008), “A modeling approach for large spatial datasets,” *Journal of the Korean Statistical Society*, 37, 3–10.
- Stein, M. L., Chi, Z., and Welty, L. J. (2004), “Approximating likelihoods for large spatial data sets,” *Journal of the Royal Statistical Society: Series B*, 66, 275–296.

- Stewart, M. (1997), “Cholesky factorization of semidefinite Toeplitz matrices,” *Linear algebra and its applications*, 254, 497–525.
- Taylor, B. M. and Diggle, P. J. (2014), “INLA or MCMC? A tutorial and comparative evaluation for spatial prediction in log-Gaussian Cox processes,” *Journal of Statistical Computation and Simulation*, 84, 2266–2284.
- Tebbutt, W., Bui, T. D., and Turner, R. E. (2016), “Circular Pseudo-Point Approximations for Scaling Gaussian Processes,” *Advances in Approximate Bayesian Inference, NIPS 2016 Workshop*, 1–5.
- Titsias, M. (2009), “Variational learning of inducing variables in sparse Gaussian processes,” in *Artificial intelligence and statistics*, PMLR, pp. 567–574.
- Trench, W. F. (1964), “An algorithm for the inversion of finite Toeplitz matrices,” *Journal of the Society for Industrial and Applied Mathematics*, 12, 515–522.
- Vecchia, A. V. (1988), “Estimation and model identification for continuous spatial processes,” *Journal of the Royal Statistical Society. Series B*, 50, 297–312.
- Wise, J., Caprio, J., and Parks, T. (1976), “Maximum likelihood pitch estimation,” *IEEE Transactions on Acoustics, Speech, and Signal Processing*, 24, 418–423.
- Wood, A. T. and Chan, G. (1994), “Simulation of stationary Gaussian processes in  $[0, 1]$  d,” *Journal of computational and graphical statistics*, 3, 409–432.
- Xiong, S. (2021), “The Reconstruction Approach: From Interpolation to Regression,” *Technometrics*, 63, 225–235.
- Zhang, Y., Leithead, W. E., and Leith, D. J. (2005), “Time-series Gaussian process regression based on Toeplitz computation of  $O(N^2)$  operations and  $O(N)$ -level storage,” in *Proceedings of the 44th IEEE Conference on Decision and Control*, IEEE, pp. 3711–3716.